



# An ENSO-induced aerosol dipole in the west-central Pacific and its potential feedback to ENSO evolution

Li Xu<sup>1</sup> · Jin-Yi Yu<sup>1</sup>

Received: 1 May 2018 / Accepted: 6 September 2018 / Published online: 12 September 2018  
© Springer-Verlag GmbH Germany, part of Springer Nature 2018

## Abstract

We examine the impact of El Niño–Southern Oscillation (ENSO) on satellite observed aerosol optical depths (AODs) over the equatorial Pacific. AODs are found to decrease close to the International Dateline and increase in the vicinity of the Maritime Continent during the El Niño developing phase (and vice versa during La Niña) to form an AOD dipole. The positive AOD anomaly over the Maritime Continent is caused by increases in fire-induced fine smoke aerosols in Indonesia and coarse dust particles transported from Australia via the strengthening winds when El Niño develops and affects the Pacific walker circulation. The negative AOD anomaly around the International Dateline is caused by decreases in the emission of marine aerosols, as the developing El Niño is associated with weakening surface wind speeds in the region. This aerosol dipole is found particularly strong during the Central-Pacific type of ENSO, which has most of its sea surface temperature and wind variations around the International Dateline. The Eastern-Pacific type of ENSO produces positive AOD anomalies over the Maritime Continent but weaker negative AOD anomalies near the International Dateline. As a result, the AOD dipole is less obvious during the EP ENSO. The shortwave radiative forcing associated with the aerosol dipole is 29% (21%) as large as the ENSO-induced outgoing longwave radiation in the Maritime Continent (International Dateline) region and represents an important positive feedback to help sustain the ENSO development that may be potentially important in Central Pacific ENSO studies and predictions.

**Keywords** Aerosol dipole · ENSO · Aerosol shortwave radiative forcing · Outgoing longwave radiation · Equatorial Pacific

## 1 Introduction

The El Niño–Southern Oscillation (ENSO) is an interannual climate variation that is characterized by positive sea surface temperature (SST) anomalies in the central-to-eastern Pacific during its El Niño phase and negative SST anomalies during its La Niña phase. These SST anomalies can alter the atmospheric circulation and excite teleconnection patterns (Bjerknes 1969; Enfield 1989) that impact regional and global climate. For instance, during an El Niño event, the anomalous warm waters in the eastern Pacific can displace atmospheric deep convection eastward, resulting in increased subsidence and drought in the western Pacific and Maritime Continent. Such changes in ambient meteorology fields can alter the production and distribution

of atmospheric trace gases and aerosols in the equatorial Pacific (Li et al. 2011; Wu et al. 2013; Xu et al. 2015, 2016; Inness et al. 2015) and over adjacent continental regions (Liu et al. 2013; Abish and Mohanakumar 2013; Xu et al. 2017; Zhao et al. 2018). The aerosols can then impact the regional climate directly by reflecting incoming solar radiation back to space or indirectly by altering cloud microphysical properties that result in changes in cloud albedo (Twomey 1974) and lifetime (Albrecht 1989). These aerosol radiative effects may be large enough to alter SSTs in the Pacific and thereby impact the development of ENSO. It has been noticed that the central location of ENSO has shifted from the Eastern Pacific (EP) to central Pacific (CP) in the past two or three decades (Lee and McPhaden 2010; Yu et al. 2012). These two types of ENSO are referred to as the EP and CP ENSO respectively (Yu and Kao 2007; Kao and Yu 2009). They differ from each other not only in the locations of their SST anomalies but also in the patterns of their associated surface wind anomalies. Therefore, these two types of ENSO possibly exert different impacts on atmospheric trace gases

✉ Li Xu  
lxu16@uci.edu

<sup>1</sup> Department of Earth System Science, University of California, Irvine, CA 92697, USA

and aerosols' abundance. A recent study, for example, finds that different La Niña types can produce contrasting influences on aerosol concentration over eastern China (Feng et al. 2017).

Previous studies have investigated the influence of ENSO on fire-induced smoke aerosols in the vicinity of the maritime continent (Chandra et al. 1998, 2009; Duncan et al. 2003; Podgorny et al. 2003; van der Werf et al. 2006; Logan et al. 2008; Chrastansky and Rotstayn 2012; Inness et al. 2015; Chen et al. 2017) as well as their feedback on regional hydrologic cycle (Rosenfeld 1999; Ramanathan et al. 2001; Chung and Ramanathan 2003; Chung et al. 2002; Rotstayn et al. 2012). ENSO can have an influence on biomass burning aerosols over the northern part of South America (Le Page et al. 2008), dust aerosols in Australia (Mitchell et al. 2010; Rosenfeld et al. 2010, 2011) and in Eastern Asia (Gong et al. 2006), winter Haze in Eastern Asia (Zhao et al. 2018), sea salt and DMS-associated sulfate aerosols in the tropic Pacific (Penner et al. 2001; Xu et al. 2015, 2016). Studies have also suggested that the radiative forcing associated with aerosols has the capability to perturb atmospheric circulation or SSTs and thereby feedback on ENSO dynamics (Wang 2007; Rotstayn et al. 2012; Xu et al. 2016; Takahashi and Watanabe 2016; Yang et al. 2016). Wang (2007) demonstrated that black carbon aerosols (e.g. from biomass burning) can exert a significant change on the atmospheric circulation and precipitation in tropics via its direct radiative effect and may enhance the warm phase of ENSO. Rotstayn et al. (2012) showed that dust aerosols can intensify the ENSO-related rainfall variability over the eastern Australia through the increase (decrease) of surface evaporation in La Niña (El Niño) years. Xu et al. (2016) showed that both sea salt and dimethyl sulfide-associated sulfate aerosols can contribute to alter the ENSO variability. Takahashi and Watanabe (2016) showed that sulfate aerosol forcing was critically contributed to changes in the tropical Pacific SST (i.e., La Niña-like cooling in the eastern Pacific) and the intensification of the Pacific easterly trade winds over the past two decades. Using two 150-year model simulation with and without interactive sea salt aerosol emissions, Yang et al. (2016) show ENSO-induced variations in sea salt aerosol emissions lead to subsequent changes in aerosol optical depth and radiative fluxes, contributing to enhance ENSO variability.

We are aware of a previous study that reported a center of aerosol anomalies over the central Pacific during ENSO events (Inness et al. 2015), but are not aware of any studies that noticed the existence of an aerosol dipole over the region close to the International Dateline (DL) and Maritime Continent (MC) during ENSO events. In this study, we show with satellite observations that such an aerosol dipole is evident during recent El Niño events, explain how the dipole is produced and why it is stronger for the Central Pacific than

the Eastern Pacific type of El Niño. We also discuss the possible influence of the aerosol dipole on the subsequent development of El Niño.

## 2 Data and analysis methods

To study the ENSO-related aerosol anomalies, we use monthly Level-3 aerosol optical depth products provided by the moderate-resolution imaging spectroradiometer (MODIS) collected from the Terra platform during the period from March 2000 to September 2016 (collection 5.1). This collection of MODIS AOD product was thoroughly evaluated for the Southeast Asia region (Reid et al. 2013) and was found to be in fairly well agreement with ground-based measurements. Here we combine the aerosol optical depth using the Deep Blue algorithm (Hsu et al. 2006) over bright surfaces with the existing MODIS algorithm over dark surfaces to derive AOD over the entire land area (Levy et al. 2007a, b). It should be noted that the use of two different algorithms for compiling the AOD information is less critical for the Southeast Asia than for other arid or elevated regions (Sayer et al. 2014). The availability of the MODIS observation is sufficiently long to cover major ENSO episodes starting from 2000. In order to include the El Niño event of 1997/1998, we also use the AOD data from the Sea-viewing Wide Field-of-view Sensor (SeaWiFS).

The meteorological variables used in this study include monthly SST and 10-m wind speed taken from the National Centers for Environmental Prediction–National Center for Atmospheric Research (NCEP–NCAR) Reanalysis 1 dataset (Kalnay 1996) as well as interpolated outgoing longwave radiation (OLR) data at the top of atmosphere (Liebmann and Smith 1996) provided by the National Oceanic and Atmospheric Administration (NOAA). Our analyses focus on the tropical Pacific region between 30°S–30°N and 90°E–60°W. The Niño 3.4 index taken from the NOAA is used to represent the strength of ENSO. Anomalies in this study are defined as the deviations from the monthly climatology values.

## 3 Results

### 3.1 Identification of an aerosol dipole

ENSO events typically reach their peak intensity during boreal winter (Rasmusson and Carpenter 1982). Thus, winter values of the Niño 3.4 index are often used to represent the overall intensity of an ENSO event. A calculation of the correlations between the December–January–February (DJF) values of the Niño 3.4 index and the AOD anomalies in the preceding and following seasons during 2000–2016

reveals large positive values over the MC region and large negative values over the DL region during the developing phase of ENSO. Here the developing and decaying phases are defined as the periods of time, respectively, before and after ENSO events reach their peak intensity during boreal winter. As an example, Fig. 1a displays the correlation pattern calculated with the September–October–November (SON) values of the AOD anomalies. The pattern indicates that the AOD increases during El Niño years over the MC region and decreases over the DL region, and vice versa for La Niña years. This seesaw-like AOD variation is defined here as the aerosol dipole. This dipole is found to be the strongest during the fall season preceding the winter (DJF) Niño 3.4 index as revealed in Fig. 1b, where the correlations with the winter Niño 3.4 index were calculated for the AOD anomalies averaged over the MC and DL regions from the preceding spring to the following fall. The figure shows that AOD correlations with Niño 3.4 are large and out of phase between the MC and DL regions only during the developing but not the decaying phases of the ENSO.

During the developing fall season, the magnitudes of the AOD correlations with the winter Niño 3.4 index in both MC and DL regions are larger than 0.7, suggesting that the ENSO explains roughly 50% of the AOD variance in these two regions during that season. These high correlations suggest that ENSO is a significant and important factor in the AOD variability in both the MC and DL regions during the developing fall. The negative correlation in the DL region first appears during the spring, starts to increase and stays high from summer to fall, but begins decreasing during the peak phase of ENSO (i.e., DJF). On the other hand, the positive correlation in the MC region first appears during summer of the developing phase of ENSO, reaches its peak during fall and begins decreasing during the early winter of the peak phase of ENSO. The different initiation time

and evolution of the AOD correlations in the DL and MC regions suggests that different mechanisms are involved in the formation of two centers of the aerosol anomaly dipole.

### 3.2 Formation mechanism of the aerosol dipole

To explore the underlying mechanisms that enable ENSO to influence AOD variations in the DL and MC regions, we regressed tropical Pacific SST anomalies onto the AOD anomalies in these two regions during the period 2000–2016. It should be noted that we have reversed the sign of AOD anomalies in the regression with the DL region to facilitate the discussion of the SST anomalies associated with the aerosol dipole. The regression shows that the negative AOD anomalies in the DL region (Fig. 2a) are associated with positive SST anomalies that first appear in the northeastern subtropical Pacific off the coast of Baja California (i.e., Lags  $-7$ ), then extend southwestward into the central equatorial Pacific (i.e., Lags  $-6$  to  $-3$ ), and finally intensify near the DL region (i.e., Lags  $-2$  to  $4$ ). This SST evolution pattern is similar to the typical evolution during the CP El Niño (Yu and Kao 2007; Kao and Yu 2009; Yu et al. 2012) and the El Niño Modoki II (Wang and Wang 2013; Wang et al. 2018). The AOD anomaly in the DL region reaches its largest magnitude (i.e., Lag 0) right before the CP El Niño peaks (around Lags 2–4 of Fig. 2a). During the development of the CP El Niño, anomalous westerlies appear resulting in a decrease in surface wind speeds over the DL region (see the contour lines overlaid in Fig. 2a). The weakened winds reduce the aerosol emissions from the ocean and result in a negative AOD anomaly in this region during the developing phase of ENSO. We performed a correlation analysis similar to that shown in Fig. 1b between 10-m winds in the DL region and the DJF Niño3.4 index shown in Fig. 3a and find their correlation to be 0.81 throughout the lifecycle of

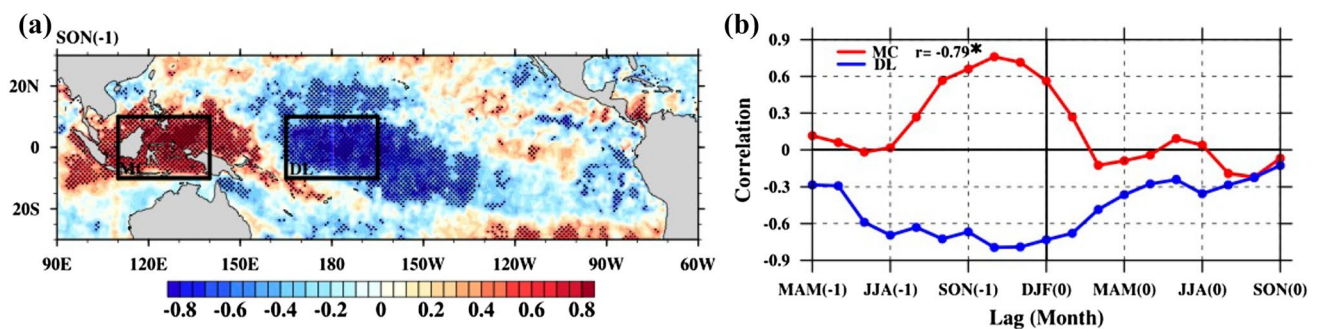


**Fig. 1** **a** The correlation between MODIS-derived AOD anomalies during September–October–November (SON) of the developing phase of ENSO and the December–January–February (DJF) Niño 3.4 index in the Tropical Pacific (30°S–30°N; 90°E–60°W) for the period 2000–2016. Two regions marked with black rectangular boxes are the Marine Continent (10°S–10°N; 110°E–140°E) and the area near the

international dateline (10°S–10°N; 165°E–195°E), and are labeled as MC and DL. **b** The lagged correlation between AOD anomalies in MC and DL and the DJF Niño 3.4 index. Statistically significant correlations (at the 95% level) in **a** are stippled. The “ $-1$ ” and “ $0$ ” in the x-axis label in **b** represent the preceding and following year, respectively

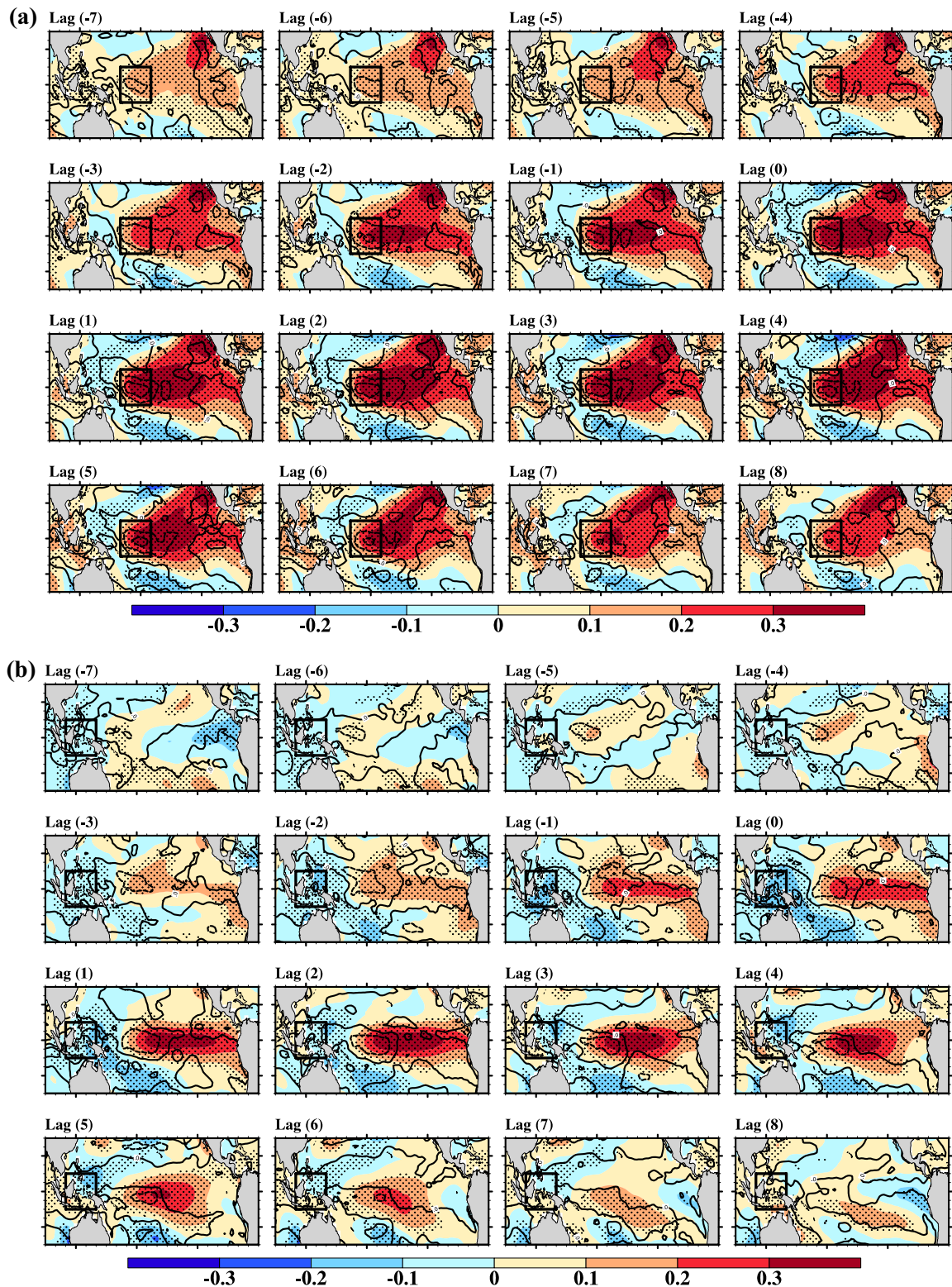


**Fig. 2** SST anomalies regressed onto the normalized AOD anomalies in the DL (a) and MC (b) regions, from 7 months before to 8 months after each specific monthly AOD anomaly during 2000–2016. The contour lines of 10-m wind speed anomalies regressed onto the normalized AOD anomalies in each region are overlaid on each panel. The solid and dashed contour lines represent positive and negative

values, respectively. Two black rectangular boxes are marked for each region. Note that the sign of AOD anomalies in the regression with the DL region in **a** has been reversed to facilitate the discussion of the SST anomalies associated with the aerosol dipole. The stippled marks the regions where SST regressions onto the normalized AOD anomalies are statistically significance at the 95% level using a student t test

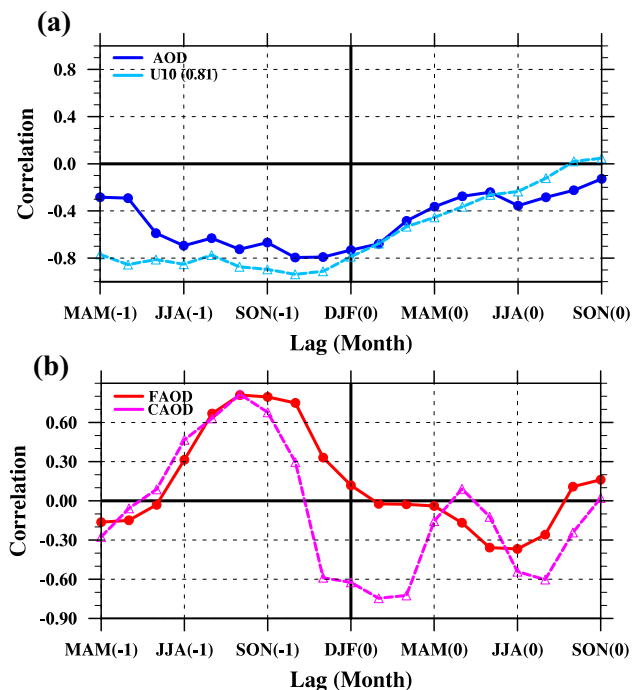


**Fig. 3** As Fig. 1, except for **a** the 10-m wind speed (U10) anomalies in the dateline (DL) region from the NCAR/NCEP dataset and **b** the fine (FAOD) and coarse aerosol optical depth (CAOD) anomalies over the marine continent (MC) during the period 2000–2016. The lagged correlation for AOD anomalies in the DL region shown in Fig. 1 is overlaid as a solid blue line. The correlation between the blue and light blue solid lines is given in the legend

the ENSO [i.e., from MAM (−1) to SON(0)]. This high correlation implies that the ENSO-induced AOD variation in the DL region composed of marine aerosols (e.g., sea salt) is predominantly explained by surface wind variations. This result is in a good agreement with the mechanism reported in Li et al. (2011) and Xu et al. (2015), where they suggested that surface winds serve as a major contributor to influence sea-salt production and aerosol transport in the tropical Pacific during El Niño events.

On the other hand, when SST anomalies are regressed onto AOD anomalies in the MC region (Fig. 2b), positive SST anomalies first appear mostly off the South American coast (e.g., Lags −7 to −4), then spread westward along the equatorial Pacific (i.e., Lags −3 to −1), and finally intensify with large SST anomalies covering the eastern-to-central Pacific (i.e., Lags 0–3). This evolution of SST anomalies appears close to the typical evolution pattern of the EP El Niño (Yu and Kao 2007; Kao and Yu 2009; Yu et al. 2012). However, we notice that the regressed SST anomalies also show some CP El Niño characteristics. Positive SST anomalies can be seen off Baja California in the early lags of the regression (e.g., Lags −7 to −5), which later spread southwestward into the tropical central Pacific. As mentioned, this is a feature during the typical developing of the CP El Niño.

Also for a typical EP El Niño, the warm SST anomalies should retreat back to the South American Coast during the decaying phase (Kao and Yu 2009; Paek et al. 2017), but this feature is not found in Fig. 2b. Instead, the decaying SST anomalies linger in the central Pacific, which is a feature typical of a decaying CP El Niño (Kao and Yu 2009; Paek et al. 2017). Therefore, the AOD anomalies in the MC region are related to both the EP and CP types of El Niño. In other words, both types of El Niño can induce AOD anomalies in the MC region.

The large SST anomalies in tropical eastern-to-central Pacific are capable of weakening the Pacific Walker circulation to increase the occurrence of droughts and fires in the MC region (Duncan et al. 2003; Podgorny et al. 2003; van der Werf et al. 2006; Chrastansky and Rotstayn 2012; Inness et al. 2015; Chen et al. 2017). In addition, drought can increase dust aerosol emissions from Australia during fall (Rotstayn et al. 2010) while the ENSO-induced meridional teleconnection can increase Asia dust during spring (Gong et al. 2006). This is in accordance with our finding that both the fine AOD (from smoke aerosols) and coarse AOD (from dusts) in the MC region increases as the Niño 3.4 index increases. As shown in Fig. 3b, the strongest correlation of the fine AOD with Niño 3.4 occurs in SON, which is the season right after the dry season (i.e., the June–July–August) of the MC region and is known to be the favorable time for fires (Chen et al. 2017). This is one reason why the aerosol dipole is strongest during the fall of the developing ENSO. In addition, the strongest correlation of the coarse AOD with Niño 3.4 also occurs in the late summer and early fall, and is related to the transport of increased dust emissions from the drought-impacted Australia to the MC region by the southerly winds of the winter monsoon season (i.e., the June–July–August). The increase in the AOD anomalies in the MC region can be produced not only by the increased aerosol emission from dry land but also via the decreased wet deposition through reduced precipitation and vice versa for the DL region during the developing phase of ENSO (Xu et al. 2016). In other words, the ENSO-induced changes in the precipitation have important effects on both aerosol surface emissions and depositions over dry land and aerosol removal processes over oceans. Thus ENSO can trigger an aerosol-induced feedback by affecting aerosol loading or the associated atmospheric circulation depending on the regions (Kim et al. 2016; Lau 2016).

As discussed above, while the MC center of the aerosol anomalies can be induced by both the EP and CP types of El Niño, the DL center of the aerosol anomalies is more closely associated with the CP type of El Niño. Therefore, the aerosol dipole appears more clearly during CP El Niño events. To further confirm the different relationships between these two types of El Niño and the aerosol dipole, we examined the AOD anomalies during three EP El Niño events

(1997–1998, 2006–2007, 2015–2016) and three CP El Niño events (2002–2003, 2004–2005, 2009–2010). The types of these events were identified using the consensus method of Yu et al. (2012). It should be noted that the 2015/2016 El Niño event is not a pure EP type of El Niño (like the 1997/1998 event is) but has a mixture of some signatures of the CP El Niño (Paek et al. 2017). Figure 4a displays the AOD anomalies during the developing fall [i.e., SON(-1)]

of these El Niño events. The most obvious feature is that all three EP events (the left panel of Fig. 4a) are associated with strong positive AOD anomalies in the MC region but relatively small negative AOD anomalies in the DL region, while all three CP events (the right panel of Fig. 4a) are associated with AOD anomalies of comparable magnitude in both MC and DL regions with opposite signs. To better compare the relative amplitudes of the AOD anomalies in

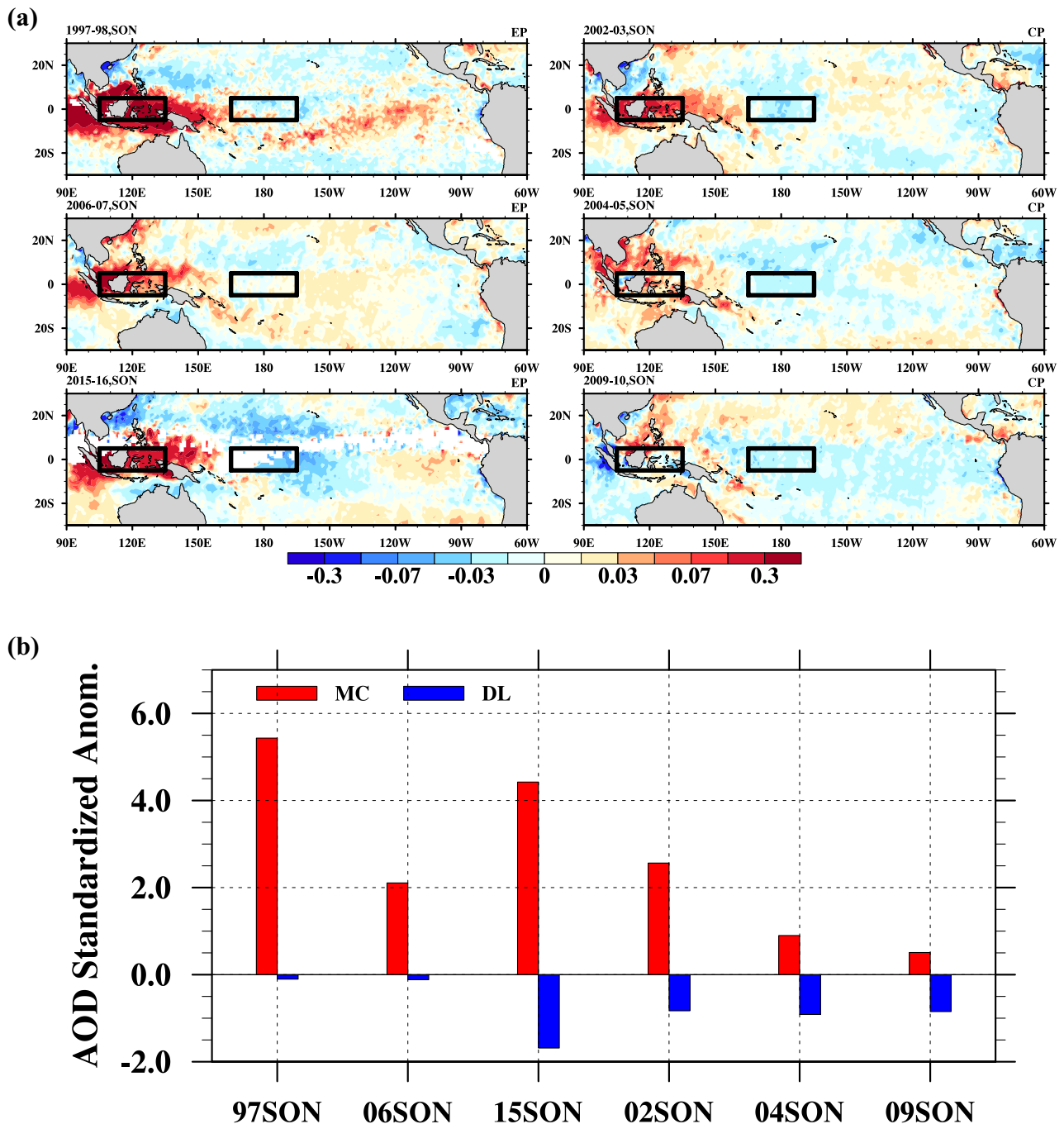


**Fig. 4** a Aerosol optical depth (AOD) anomalies in the tropical Pacific during the fall (SON) prior to the peak of the six ENSO events and b average standardized AOD anomalies in the DL and MC region during six ENSO events

these two regions, we show in Fig. 4b the AOD anomalies normalized by their standard deviation in each region for all El Niño events. The results in Fig. 4b confirm that EP El Niño events produce much larger AOD amplitude in the MC region than in the DL, while the AOD anomalies are comparable between the two regions for the CP El Niño events. Only the 2015–2016 EP El Niño also shows relatively large AOD anomalies in the DL region, which supports the suggestion of Paek et al. (2017) that this El Niño event has characteristics of both the EP and CP types of El Niño. We find the AOD differences between the MC and DL regions to be statistically significant (at the 95% level using a Student t test) for the four CP ENSO events but not significant for the two EP ENSO events. The AOD differences are still significant when all six events (i.e., both the EP and CP events) are considered together. Figure 4b confirms that the aerosol dipole is more closely associated with the CP than EP type of El Niño. A correlation analysis of AOD anomalies with the Niño 1 + 2, Niño 3 and Niño 4 indices shown in Fig. 5 further confirms that the aerosol dipole appears more clearly when the characteristic center of SST anomalies shifts from the eastern Pacific (i.e., the Niño 1 + 2 region) to the central Pacific (i.e., the Niño 4 region).

### 3.3 Potential feedback of the aerosol dipole on ENSO evolution

As mentioned, aerosols can impact local climate via radiative processes. It is possible that the aerosol dipole induced by ENSO may feedback to affect its subsequent evolution. Figure 2 shows that SST anomalies are positive in the DL region but negative in the MC region during the developing phase of the El Niño. The decreased AOD in the DL region can result in an increase in the amount of shortwave radiative flux into the ocean that helps maintain the positive SST

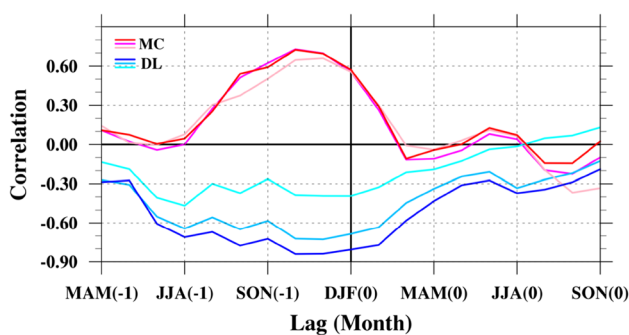


**Fig. 5** Similar to Fig. 1, except for the lagged correlation between AOD anomalies over the marine continent (MC) and the dateline (DL) and the DJF Niño 1 + 2 (pink solid line for MC and cyan solid line for DL), Niño 3 (magenta solid line for MC and light blue solid line for DL), and Niño 4 indices (red solid line for MC and blue solid line for DL)

anomalies, while the increased AOD in the MC region can help maintain the negative SST anomalies by decreasing the downward shortwave radiative fluxes. We illustrate in Fig. 6 the mechanism that may enable the aerosol dipole over the marine continent (MC) and the dateline (DL) regions during the developing phase of ENSO to influence the subsequent ENSO evolution. Through this mechanism, the aerosol dipole may produce a positive feedback to SST anomalies in both the MC and DL regions. In other words, the warmer SSTs in the DL region become warmer while the colder SSTs in the MC region become colder. This feedback helps increase the SST gradient between MC and DL regions, slowing the decay of SST anomalies during El Niño events and therefore contributing to maintain the El Niño. This positive feedback on SSTs from the aerosol dipole is similar to those produced by DMS-associated sulfate (Xu et al. 2016) and sea salt aerosols (Yang et al. 2016) but has a more profound influence in ENSO evolution. To gain a more quantitative insight into the importance of this feedback to the ENSO evolution, we compared the shortwave aerosol radiative forcing (SARF) anomalies associated with the dipole to the outgoing longwave radiation (OLR) anomalies typically found during El Niño. The OLR is noted to provide a good proxy for atmospheric deep convection and exhibits unique characteristics in the equatorial Pacific during El Niño events (Chiodi and Harrison 2010, 2013). Here the SARF is defined as the clear-sky shortwave aerosol forcing at the top of atmosphere in a region of interest over oceans (Christopher et al. 2000). The SARF is estimated from MODIS retrievals following the method of Christopher and Zhang (2002), which relates the cloud-free SARF over the oceans to the values of AOD with a simple polynomial equation:  $SARF = 0.35 - 105.34 \tau_{550} + 61.47 \tau_{550}^2$  where  $\tau_{550}$  is the aerosol optical depth at the wavelength of 550 nm from MODIS and SARF has a unit of  $W m^{-2}$ . It should be noted that this simple calculation of SARF may be considered as

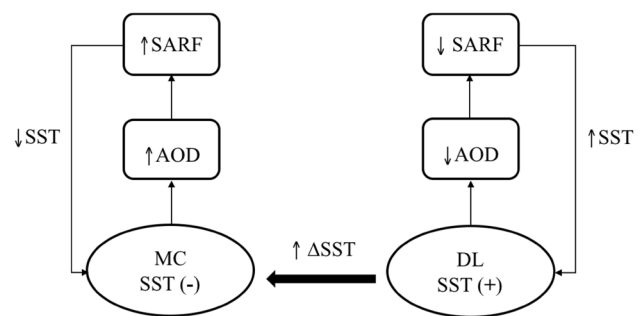


**Fig. 6** The diagram illustrates the mechanism that enables the aerosol dipole over the marine continent (MC) and the dateline (DL) regions during the developing phase of ENSO to influence the subsequent ENSO evolution. The “+” and “-” represent positive and negative anomalies, respectively. The “↑” and “↓” represent increasing and decreasing tendency, respectively

a first-order approximation because the SARF is not only determined by aerosol loadings but also dependent upon other factors (e.g., aerosol types with some species scattering sunlight and some absorbing sunlight, cloud fraction, etc.). Since the SARF only applies to the aerosol radiative forcing in cloud-free conditions, the indirect aerosol forcing related to clouds is not included. The SARF estimated here may be smaller than the total shortwave radiative forcing that includes both the direct and indirect effects of aerosols. We calculated the regression coefficients of the SARF and OLR anomalies along the equatorial Pacific ( $10^{\circ}\text{S}$ – $10^{\circ}\text{N}$ ) onto the Niño 3.4 index during SON(–1). The results are shown in Fig. 7a. It should be noted that, for the sake of better comparison of amplitudes of ENSO-induced OLR and SARF, we reversed the sign of regression coefficients of OLR with respect to the Niño 3.4 index such that positive values of both OLR and SARF in the figure are considered to have positive impacts on SSTs, and vice versa.

As shown in Fig. 7a and Table 1, a developing El Niño increases the upward OLR (i.e., negative anomaly values in the figure) by about  $7.3 \text{ W m}^{-2}$  per unit of Niño 3.4 index over the MC region (where the El Niño-induced anomalous descending motions suppress deep convection and allow more longwave radiation to escape at the top of the atmosphere) but decreases by a roughly similar amount the upward OLR (i.e., positive anomaly values in the figure) extending from the DL region to the eastern Pacific (where the El Niño-induced anomalous ascending motions encourage deep convection and allow less longwave radiation to escape at the top of the atmosphere). The increased upward OLR anomalies over the MC region can cool the local SSTs, while the decreased upward OLR anomalies over the DL region can warm the local SSTs. Therefore, the OLR anomalies contribute to maintain negative SST anomalies in the

**Table 1** The regionally averaged regression coefficients (unit:  $\text{W m}^{-2}$  per unit of Niño 3.4) of the shortwave aerosol radiative forcing (SARF) and the outgoing longwave radiation (OLR) anomalies regressed onto the DJF Niño 3.4 index in the MC and DL region and their ratios

Region	SARF ( $\text{W m}^{-2}$ )	OLR ( $\text{W m}^{-2}$ )	Ratio (SARF/OLR)
MC	–2.15	–7.32	0.29
DL	1.58	7.37	0.21

MC region and positive SST anomalies in the DL region as shown in Fig. 6, which represents a positive feedback that helps sustain the El Niño. The same figure shows that the aerosol dipole produces negative SARF of about  $-2.2 \text{ W m}^{-2}$  per unit of Niño 3.4 index in the MC region and comparably smaller SARF in the DL region, which also represents a positive radiative feedback on SSTs. This positive feedback could potentially result in a positive SST gradient from the DL region to the MC region that helps sustain the El Niño. The magnitudes of the SARF in the MC and DL regions are roughly 29% and 21% of those of the OLR, respectively, suggesting that the radiative feedback from the aerosol dipole may be of a similar order of magnitude as that of the OLR and could be a potentially important factor influencing the development of ENSO. As aforementioned, aerosols can have an influence on regional or local climate through their indirect effects on cloud morphology and lifetime besides the direct aerosol effect estimated here. Thus, it is expected that the influence of the aerosol dipole on SSTs could be more or less than that estimated here. Nevertheless, the SARF provides a useful first-order estimate of the impact of the aerosol dipole on ENSO.

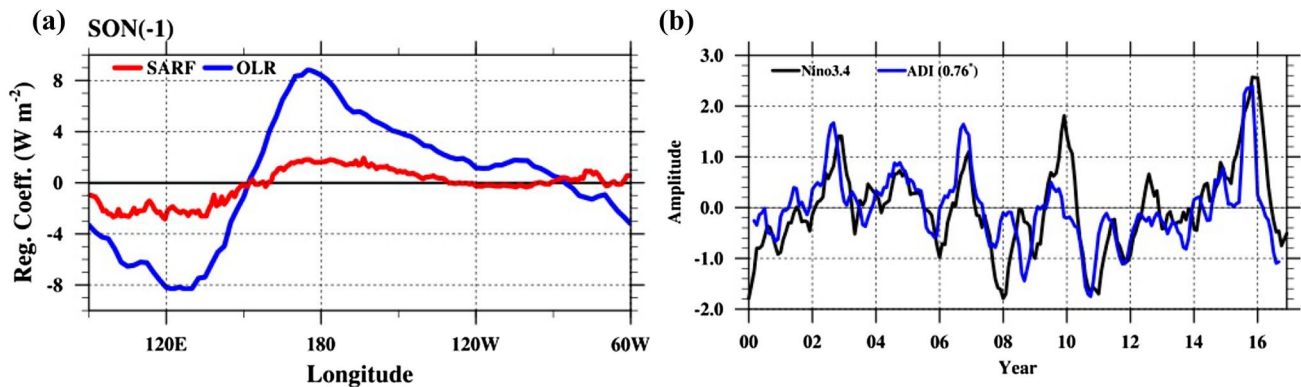


**Fig. 7** **a** The regression coefficients of the shortwave aerosol radiative forcing (SARF) and the outgoing longwave radiation (OLR) anomalies regressed onto the DJF Niño 3.4 index and **b** the time series of the aerosol dipole index (ADI) and the Niño 3.4 index during the period 2000–2016. The sign of regression coefficients of OLR

with respect to the Niño 3.4 index is reversed in **a**. The correlation between the ADI and the Niño 3.4 index is provided in the legend in **b** and the star symbol presents that the correlation exceeds the 95% significance level

We further constructed an aerosol dipole index (ADI) by subtracting the AOD anomalies in the DL region from those in the MC region and then normalizing the difference. A 5-month running mean was applied to the time series of this aerosol dipole index. As shown in Fig. 7b, the aerosol dipole index follows closely the variations in the Niño 3.4 index but tends to peak about 2 months earlier than the Niño 3.4 index. The correlation coefficient between the Niño 3.4 index and the aerosol dipole index at a lag of minus two months is 0.76, which exceeds the 95% significance level. Since the aerosol dipole index leads the Niño 3.4 index, the aerosol index may be potentially useful in predicting how soon or late that an El Niño or La Niña event may terminate as a complimentary to oceanic indices.

## 4 Conclusions

We have shown via observational analyses that an aerosol dipole in the equatorial Pacific can be induced by ENSO. This aerosol dipole, which is characterized with positive AOD anomalies over the MC region and negative AOD anomalies over the DL region, is strongest during the fall prior to the peak of El Niño, particularly in the CP type of El Niño. Each center of the aerosol dipole, although is composed of different aerosol species and formed via distinct mechanisms, is capable of producing a positive feedback to help maintain the SST anomalies associated with ENSO. The shortwave radiative forcing induced by the aerosol dipole has a magnitude comparable (though somewhat smaller) to that of the outgoing longwave radiation induced by ENSO. Since ENSO has changed from the EP to the CP type in recent decades (Kao and Yu 2009; Lee and McPhaden 2010; Yu et al. 2012) and the CP type is likely to continue to occur more frequently in the future, the aerosol dipole and its feedback to the evolution of ENSO may be potentially important in Central Pacific ENSO studies and prediction frameworks.

**Acknowledgements** We thank two anonymous reviewers for their valuable comments. This research was supported by the National Science Foundation's Climate and Large Scale Dynamics Program under Grant AGS-1505145. L. X. is grateful for the support from the Department of Energy's Earth System Modeling Program under Grant DE-SC0016362. The MODIS aerosol optical depth data is downloaded from <https://ladsweb.modaps.eosdis.nasa.gov>, the SeaWiFS aerosol optical depth data from [https://measures.gsfc.nasa.gov/data/DeepBlueSeaWiFS\\_Level3/](https://measures.gsfc.nasa.gov/data/DeepBlueSeaWiFS_Level3/), the NCEP/NCAR Reanalysis data set, the outgoing longwave radiation data and the Niño 3.4 index from <https://www.esrl.noaa.gov/psd/>.

## References

Abish B, Mohanakumar K (2013) Absorbing aerosol variability over the Indian subcontinent and its increasing dependence on ENSO. *Glob Planet Change* 106:13–19

- Albrecht BA (1989) Aerosols, cloud microphysics, and fractional cloudiness. *Science* 245:1227–1230
- Bjerknes J (1969) Atmospheric teleconnections from the equatorial Pacific. *Mon Weather Rev* 18:820–829
- Chandra S, Ziemke JR, Min JR, Read WG (1998) Effects of 1997–1998 El Niño on tropospheric ozone and water vapor. *Geophys Res Lett* 25:3867–3870. <https://doi.org/10.1029/98GL02695>
- Chandra S, Ziemke JR, Duncan BN, Diehl TL, Livesey NJ, Froidevaux L (2009) Effects of the 2006 El Niño on tropospheric ozone and carbon monoxide: implications for dynamics and biomass burning. *Atmos Chem Phys* 9:4239–4249. <https://doi.org/10.5194/acp-9-4239-2009>
- Chen Y, Morton DC, Andela N, van der Werf GR, Giglio L, Randerion JT (2017) A pan-tropical cascade of fire driven by El Niño/Southern oscillation. *Nat Clim Change* 7:906–911
- Chiodi AM, Harrison DE (2010) Characterizing warm-ENSO variability in the equatorial Pacific: an OLR perspective. *J Clim* 23:2428–2439
- Chiodi AM, Harrison DE (2013) El Niño impacts on seasonal U.S. atmospheric circulation, temperature, and precipitation anomalies: the OLR-event perspective. *J Clim* 26:822–837. <https://doi.org/10.1175/JCLI-D-12-00097.1>
- Chrastansky A, Rotstain LD (2012) The effect of ENSO-induced rainfall and circulation changes on the direct and indirect radiative forcing from Indonesian biomass-burning aerosols. *Atmos Chem Phys* 12:11395–11416. <https://doi.org/10.5194/acp-12-11395-2012>
- Christopher SA, Zhang J (2002) Shortwave aerosol radiative forcing from MODIS and CERES observations over the oceans. *Geophys Res Lett* 29(18):1859. <https://doi.org/10.1029/2002GL014803>
- Christopher SA, Chou J, Zhang J, Li X, Welch RM (2000) Shortwave direct radiative forcing of biomass burning aerosols estimated from VIRS and CERES. *Geophys Res Lett* 27:2197–2200
- Chung CE, Ramanathan V (2003) South Asian haze forcing: remote impacts with implications to ENSO and AO. *J Clim* 16:1791–1806
- Chung CE, Ramanathan V, Kiehl JT (2002) Effects of the South Asian absorbing haze on the northeast monsoon and surface-air heat exchange. *J Clim* 15:2462–2476
- Duncan BN, Bey I, Chin M, Mickley LJ, Fairlie TD, Martin RV, Matusueda H (2003) Indonesia wildfires of 1997: impact on tropospheric chemistry. *J Geophys Res* 108:4458. <https://doi.org/10.1029/2002JD003195>
- Enfield DB (1989) El Niño, past and present. *Rev Geophys* 27(1):159–187. <https://doi.org/10.1029/RG027i001p00159>
- Feng J, Li J, Zhu J, Liao H, Yang Y (2017) Simulated contrasting influences of two La Niña Modoki events on aerosol concentrations over eastern China. *J Geophys Res Atmos* 122:2734–2749. <https://doi.org/10.1002/2016JD026175>
- Gong SL, Zhang XY, Zhao TL, Zhang XB, Barrie LA, McKendry IG, Zhao CS (2006) A simulated climatology of Asian Dust aerosol and its trans-Pacific transport. Part II: interannual variability and climate connections. *J Clim* 19:104–122. <https://doi.org/10.1175/JCLI3606.1>
- Hsu NC, Tsay SC, King MD, Herman JR (2006) Deep blue retrievals of Asian aerosol properties during ACE-Asia. *IEEE Trans Geosci Remote* 44:3180–3195. <https://doi.org/10.1109/TGRS.2006.879540>
- Inness A, Benedetti A, Flemming J, Huijnen V, Kaiser JW, Parrington M, Remy S (2015) The ENSO signal in atmospheric composition fields: emission-driven versus dynamically induced changes. *Atmos Chem Phys* 15:9083–9097. <https://doi.org/10.5194/acp-15-9083-2015>
- Kalnay VE et al (1996) The NCEP/NCAR 40-year reanalysis project. *Bull Am Meteorol Soc* 77:437–471

- Kao H-Y, Yu J-Y (2009) Contrasting Eastern-Pacific and Central-Pacific types of ENSO. *J Clim* 22:615–632. <https://doi.org/10.1175/2008JCLI2309.1>
- Kim M-K, Lau WK-M, Kim K-M et al (2016) Amplification of ENSO effects on Indian summer monsoon by absorbing aerosols. *Clim Dyn* 46:2657–2671. <https://doi.org/10.1007/s00382-015-2722-y>
- Lau WKM (2016) The aerosol-monsoon climate system of Asia: a new paradigm. *J Meteorol Res* 30(1):001–011. <https://doi.org/10.1007/s13351-015-5999-1>
- Le Page Y, Pereira JMC, Trigo R, da Camara C, Oom D, Mota B (2008) Global fire activity patterns (1996–2006) and climatic influence: an analysis using the World Fire Atlas. *Atmos Chem Phys* 8:1911–1924. <https://doi.org/10.5194/acp-8-1911-2008>
- Lee T, McPhaden MJ (2010) Increasing intensity of El Niño in the central-equatorial Pacific. *Geophys Res Lett* 37:L14603. <https://doi.org/10.1029/2010GL044007>
- Levy RC, Remer LA, Dubovik O (2007a) Global aerosol optical properties and application to moderate resolution imaging spectroradiometer aerosol retrieval over land. *J Geophys Res Atmos* 112:D13210. <https://doi.org/10.1029/2006JD007815>
- Levy RC, Remer LA, Mattoo S, Vermote EF, Kaufman YJ (2007b) Second-generation operational algorithm: retrieval of aerosol properties over land from inversion of moderate resolution imaging spectroradiometer spectral reflectance. *J Geophys Res Atmos* 112:D13211. <https://doi.org/10.1029/2006JD007811>
- Li J, Carlson BE, Laciis AA (2011) El Niño–Southern Oscillation correlated aerosol Ångström exponent anomaly over the tropical Pacific discovered in satellite measurements. *J Geophys Res* 116:D20204. <https://doi.org/10.1029/2011JD015733>
- Liebmann B, Smith CA (1996) Description of a complete (interpolated) outgoing longwave radiation dataset. *Bull Am Meteorol Soc* 77:1275–1277
- Liu Y, Liu J, Tao S (2013) Interannual variability of summertime aerosol optical depth over East Asia during 2000–2011: a potential influence from El Niño–Southern Oscillation. *Environ Res Lett* 8:044034
- Logan JA, Megretskaia I, Nassar R, Murray LT, Zhang L, Bowman KW, Worden HM, Luo M (2008) Effects of the 2006 El Niño on tropospheric composition as revealed by data from the tropospheric emission spectrometer (TES). *Geophys Res Lett* 35:L03816. <https://doi.org/10.1029/2007GL031698>
- Mitchell RM, Campbell SK, Qin Y (2010) Recent increase in aerosol loading over the Australian arid zone. *Atmos Chem Phys* 10:1689–1699. <https://doi.org/10.5194/acp-10-1689-2010>
- Paek H, Yu J-Y, Qian C (2017) Why were the 2015/2016 and 1997/1998 extreme El Niños different? *Geophys Res Lett* 44:1848–1856. <https://doi.org/10.1002/2016GL071515>
- Penner JE et al (2001) Aerosols, their direct and indirect effects. In: Houghton JT et al (eds) *Climate change 2001: the scientific basis, contribution of working group I to the third assessment report of the intergovernmental panel on climate change*, Chap 5. Cambridge University Press, Cambridge, pp 289–348
- Podgorny IA, Li F, Ramanathan V (2003) Large aerosol radiative forcing due to the 1997 Indonesian forest fire. *Geophys Res Lett* 30:1028. <https://doi.org/10.1029/2002GL015979>
- Ramanathan V, Crutzen PJ, Kiehl JT, Rosenfeld D (2001) Aerosols, climate, and the hydrological cycle. *Science* 294:2119–2124. <https://doi.org/10.1126/science.1064034>
- Rasmusson EM, Carpenter TH (1982) Variations in tropical sea surface temperature and surface wind fields associated with the Southern Oscillation/El Niño. *Mon Weather Rev* 110:354–384
- Reid JS et al (2013) Observing and understanding the Southeast Asian aerosols by remote sensing: an initial review and analysis for the Seven Southeast Asian Studies (7 SEAS) program. *Atmos Res* 122:303–468. <https://doi.org/10.1016/j.atmosres.2012.06.005>
- Rosenfeld D (1999) TRMM observed first direct evidence of smoke from forest fires inhibiting rainfall. *Geophys Res Lett* 26(20):3105–3108. <https://doi.org/10.1029/1999GL006066>
- Rosenfeld D, Axisa D, Woodley WL, Lahav R (2010) A quest for effective hygroscopic cloud seeding. *J Appl Meteorol Climatol* 49(7):1548–1562. <https://doi.org/10.1175/2010JAMC2307.1>
- Rosenfeld D, Clavner M, Nirel R (2011) Pollution and dust aerosols modulating tropical cyclones intensities. *Atmos Res* 102(1–2):66–76. <https://doi.org/10.1016/j.atmosres.2011.06.006>
- Rotstayn LD, Collier MA, Dix MR, Feng Y, Gordon HB, O’Farrell SP, Smith IN, Syktus J (2010) Improved simulation of Australian climate and ENSO-related climate variability in a GCM with an interactive aerosol treatment. *Int J Climatol* 30:1067–1088. <https://doi.org/10.1002/joc.1952>
- Rotstayn LD, Jeffrey SJ, Collier MA, Dravitzki SM, Hirst AC, Syktus JI, Wong KK (2012) Aerosol- and greenhouse gas-induced changes in summer rainfall and circulation in the Australasian region: a study using single-forcing climate simulations. *Atmos Chem Phys* 12:6377–6404. <https://doi.org/10.5194/acp-12-6377-2012>
- Sayer AM, Munchak LA, Hsu NC, Levy RC, Bettenhausen C, Jeong M-J (2014) MODIS Collection 6 aerosol products: comparison between Aqua’s e-Deep Blue, Dark Target, and “merged” data sets, and usage recommendations. *J Geophys Res Atmos* 119:13965–13989. <https://doi.org/10.1002/2014JD022453>
- Takahashi C, Watanabe M (2016) Pacific trade winds accelerated by aerosol forcing over the past two decades. *Nat Clim Change* 6:768–772
- Twomey S (1974) Pollution and the planetary albedo. *Atmos Environ* 8:1251–1256
- van der Werf GR, Randerson JT, Giglio L, Collatz GJ, Kasibhatla PS, Arellano Jr AF (2006) Interannual variability in global biomass burning emissions from 1997 to 2004. *Atmos Chem Phys* 6:3423–3441. <https://doi.org/10.5194/acp-6-3423-2006>
- Wang C (2007) Impact of direct radiative forcing of black carbon aerosols on tropical convective precipitation. *Geophys Res Lett* 34(5):L05709. <https://doi.org/10.1029/2006GL028416>
- Wang C, Wang X (2013) Classifying El Niño Modoki I and II by different impacts on rainfall in Southern China and typhoon tracks. *J Clim* 26:1322–1338. <https://doi.org/10.1175/JCLI-D-12-00107.1>
- Wang X, Tan W, Wang C (2018) A new index for identifying different types of El Niño Modoki events. *Clim Dyn* 50:2753–2765. <https://doi.org/10.1007/s00382-017-3769-8>
- Wu R, Wen Z, He Z (2013) ENSO contribution to aerosol variations over the maritime continent and the Western North Pacific during 2000–10. *J Clim* 26:6541–6560. <https://doi.org/10.1175/JCLI-D-12-00253.1>
- Xu L, Pierce DW, Russell LM, Miller AJ, Somerville RCJ, Twohy CH, Ghan SJ, Singh B, Yoon J-H, Rasch PJ (2015) Interannual to decadal climate variability of sea salt aerosols in the coupled climate model CESM1.0. *J Geophys Res Atmos* 120:1502–1519. <https://doi.org/10.1002/2014JD022888>
- Xu L, Cameron-Smith P, Russell LM, Ghan SJ, Liu Y, Elliott S, Yang Y, Lou S, Lamjiri MA, Manizza M (2016) DMS role in ENSO cycle in the tropics. *J Geophys Res Atmos* 121:13537–13558. <https://doi.org/10.1002/2016JD025333>
- Xu L, Yu J-Y, Schnell JL, Prather MJ (2017) The seasonality and geographic dependence of ENSO impacts on U.S. surface ozone variability. *Geophys Res Lett* 44:3420–3428. <https://doi.org/10.1002/2017GL073044>
- Yang Y, Russell L, Lou S, Lamjiri MA, Liu Y, Singh B, Ghan S (2016) Changes in sea salt emissions enhance ENSO

- variability. *J Clim* 29:8575–8588. <https://doi.org/10.1175/JCLI-D-16-0237.1>
- Yu J-Y, Kao H-Y (2007) Decadal changes of ENSO persistence barrier in SST and ocean heat content indices: 1958–2001. *J Geophys Res* 112:D13106. <https://doi.org/10.1029/2006JD007654>
- Yu J-Y, Zou Y, Kim ST, Lee T (2012) The changing impact of El Niño on US winter temperatures. *Geophys Res Lett* 39:L15702. <https://doi.org/10.1029/2012GL052483>
- Zhao S, Zhang H, Xie B (2018) The effects of El Niño–Southern Oscillation on the winter haze pollution of China. *Atmos Chem Phys* 18:1863–1877. <https://doi.org/10.5194/acp-18-1863-2018>